RE-EVAPORATION OF ADSORBED (TOXIC) COMPOUNDS INSIDE AN ACTIVATED CARBON FILTER.

Angélique Léonard, Department of Applied Chemistry, University of Liège, B6c, Sart Tilman, 4000 Liège, Belgium
Silvia Blacher, Department of Applied Chemistry, University of Liège, B6c, Sart Tilman, 4000 Liège, Belgium
Hilda Wullens, DLD, Defense Laboratories Department, NBC Protection, Kwartier Majoor Housiau, Martelarenstraat 181, 1800 Peutie, Belgium
Michel Crine, Department of Applied Chemistry, University of Liège, B6c, Sart Tilman, 4000 Liège, Belgium
Peter Lodewyckx, Royal Military Academy, Department of Chemistry, Renaissancelaan 30, 1000 Brussel, Belgium

Introduction

Activated carbon filters are widely used to protect people from harmful substances, both in military and industrial environments. Re-using a filter, i.e. storing a filter after it has been exposed to a toxic vapour without having exhausted its full capacity in order to use it again at a later date, is in most cases prohibited by manufacturer instructions and company procedures. However, it is still common practice in many enterprises, simply based on economics and the belief that the capacity of a filter is independent of time, i.e. the sum of the amounts adsorbed at different time intervals must only stay lower than the total (dynamic) capacity of the activated carbon bed. This work focuses on the possible re-arrangement of the adsorption front inside a partially saturated activated carbon bed by a re-evaporation (i.e. local desorption) of the adsorbed compound. This has been studied by a combination of x-ray microtomography coupled to image analysis and breakthrough experiments: after an initial exposure to a chemical compound, filters were scanned at regular time intervals in an x-ray microtomograph to study the re-distribution of the compound inside the bed. Breakthrough tests of partially saturated carbon filters were carried out to evaluate the influence of this re-arrangement on breakthrough times after a defined storing period.

Experimental

Filter testing

First plastic cylinders were used to simulate gas filters. At the entry and exit a metal frame was inserted to permit the gas flow to enter and leave the filters. The diameter of the test tubes was 26 mm. Tests were conducted with 6 g of BPL® 12×30 activated carbon (Calgon Carbon Corporation). The test gas was put to the filters using a classical filter testing installation (Lodewyckx and Vansant, 1999). The air flow was 5 litres/min, corresponding to a superficial velocity in the filter of 17 cm/s. Tests were conducted at room temperature with a fixed concentration of 1000 ppm in a dry air stream of, respectively, CH_3I, CCl_4 and C_6H_5Cl. The test tubes were solicited with the contaminated air stream till one third of the, previously determined, breakthrough time. This to ensure that approximately half of the filter would be saturated, and the other half not contaminated. Microtomographic images (see below) were taken immediately after the contamination and, subsequently, at regular time intervals.

Given the short breakthrough times of the test tubes, it was very difficult to evaluate the effect of a possible re-evaporation. Therefore the same procedure was performed with filters of 9 cm diameter, filled with 78 g of the same activated carbon. After a re-equilibration period of 6 days they were tested till breakthrough with different organic vapours. These breakthrough times were then compared to those of non-contaminated filters.

X-ray microtomography

X-ray microtomography is a powerful non-invasive technique allowing the visualization of the internal texture of a sample based upon local variation of the x-ray attenuation coefficient. It was used to obtain 2-dimensional cross section images of the carbon bed. During tomographic investigation, an X-ray beam is sent on the sample and the transmitted beam is recorded with a detector. According to Beer-Lambert law, the transmitted intensity is related to the integral of the X-ray attenuation coefficient along the path of the beam, μ. This coefficient μ depends on the material density, ρ, the atomic number of the material, Z, and on the energy of the incident beam, E, according to Eq (1):

$$\mu = \rho\left(\mathrm{a} + \frac{\mathrm{b}Z^{3.8}}{E^{3.2}}\right) \qquad (1)$$

where a and b are energy-dependent coefficients (Vinegar and Wellington, 1987). Projections (defined by the assembling of transmitted beams) are recorded for several angular positions by rotating the sample between 0 and 180°. Then a back-projection algorithm is used to reconstruct 2D or 3D images, depending on the method used. In the case of 2D images, each pixel is characterized by a grey level value corresponding to the local attenuation coefficient.

The x-ray tomographic device used in this study was a "Skyscan-1074 X-ray scanner" (Skyscan, Belgium). Advanced technical details about its conception and operation are described by Sasov and Van Dyck (1998). The cone beam source operated at 40 kV and 1 mA. The detector was a 2D, 768 pixels × 576 pixels, 8-bit X-ray camera with a spatial resolution of 41 µm. The rotation step was fixed at the minimum, 0.9°, in order to improve image quality, giving total acquisition times close to 10 minutes. For each angular position a radiograph of the whole bed, instead of a 1D-projection of a cross section, was recorded by the 2D camera. In contrast to a classical medical scanner, the source and the detector were fixed, while the sample was rotated during the measurement. Once the sample was placed into the microtomograph, the scanning was performed, allowing the investigation of a height of max 25 mm. Cross sections separated by 205 µm were reconstructed along the carbon bed using a cone beam reconstruction software, based on the Feldkamp algorithm (Feldkamp, 1984).

Image analysis

Image analysis was performed using the Aphelion3.2 (Adsis) software on a PC that allowed implementing algorithms using signal processing and tools from mathematical morphology (Soille, 1999). The developed image analysis algorithm was based on the observation that the grey level intensity of the carbon grains darkens when vapour is adsorbed. Taking this into account, image analysis was performed on each cross section according to the following steps: from original grey-level image cross-section (Fig.1a), a binary mask was automatically constructed (Fig.1b) and used in order to isolate the bed from the background (Fig.1c). Next, the image was eroded to eliminate possible borders effects (Fig.1d). On this last image, the intensity, i.e. the addition of all the pixel values of the grey level image, was calculated. The intensity of the approximately 100 cross-sections images per sample was determined and the result drawn in function of the depth of the sample, i.e. the distance from the inlet of the carbon bed.

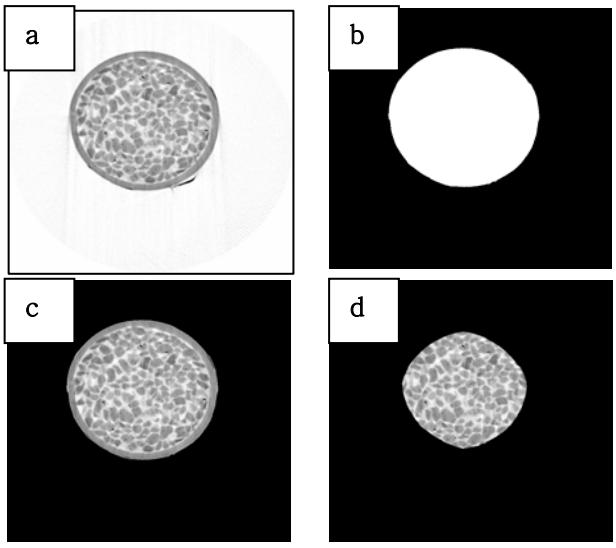

Figure 1. Example Image analysis processing - a. original cross section image b. binary mask c. elimination of background d. erosion of the image to exclude border effects.

Results & Discussion

Visualisation of the adsorption front

The adsorption front profiles in the filters, as visualised by the x-ray microtomography, are depicted in Fig 2 and 3. Fig 2 gives the long-term result for CH_3I. The Y-axis is in arbitrary intensity units (i.e. gray level), the X-axis depicts the axial coordinate of the filter from entrance to exit. At J0 (day zero, i.e. immediately after contaminating the filter till approximately one third of its breakthrough time) there is a clear adsorption front. This front flattens out over time: after three to four days the concentration of the organic vapour is equally distributed throughout the filter. The loss of CH_3I between days four and nine is due to evaporation of the vapour at the in- and outlet of the filter.

There is a marked difference between the three organic vapours: CCl_4 and CH_3I showed a similar behaviour, that of C_6H_5Cl was quite different. In Fig 3 the Y-axis does not have the same scale as in Fig 2: as some vapours give a lower intensity than others (e.g. C_6H_5Cl, see higher) the figures were blown up to show as clearly as possible the evolution of the adsorption front. After two days the adsorption front is still clearly visible for C_6H_5Cl, whereas it has almost completely vanished for CH_3I. As both CCl_4 and CH_3I show this behaviour, and C_6H_5Cl not, this is clearly linked to the vapour pressure of the organic compounds: a higher volatility facilitates desorption and thus a rearranging of molecules through the bed.

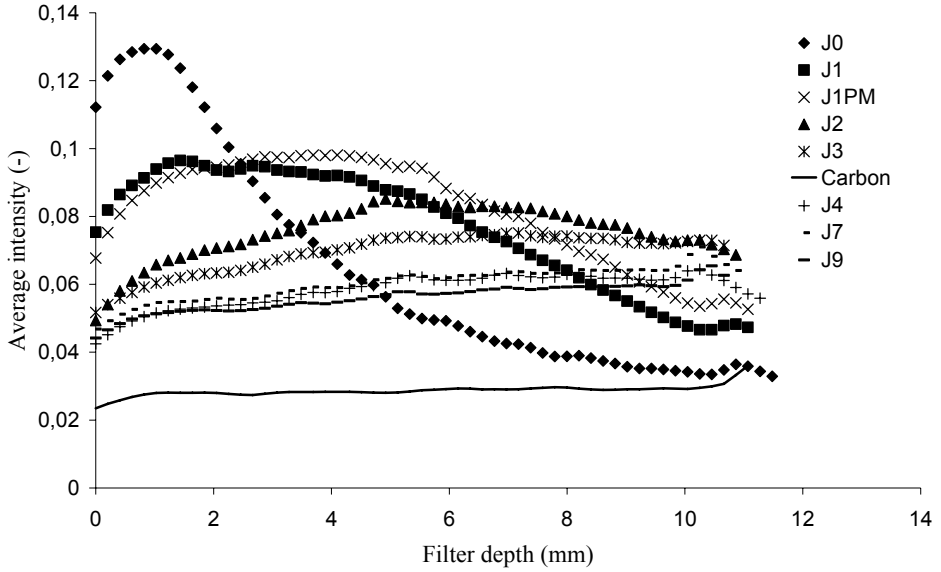

Figure 2. Re-distribution of CH_3I over time: concentration of CH_3I versus axial coordinate.

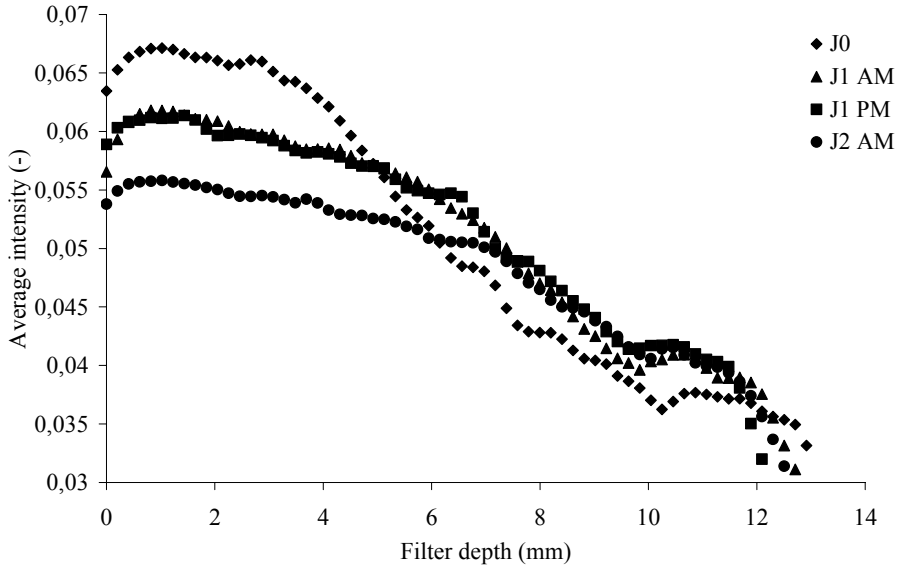

Figure 3. Re-distribution of C_6H_5Cl over time: concentration versus axial coordinate.

Breakthrough results

The results of the breakthrough tests are summarized in Table 1. The second breakthrough time was calculated as the sum of the breakthrough time of the previously contaminated and re-equilibrated filter and the contamination time. Some of the tests were performed on 'real' filters (diameter 9 cm) and others on test tubes. But the general trend is the same: the results do not show any significant influence of the re-distribution of the adsorption front on the breakthrough time of the filter: the differences are smaller than 10% and are smaller than the experimental uncertainty on the breakthrough measurement. This means filters can actually be re-used after a prior use because breakthrough times can be added up.

One should bear in mind however this only applies when the second challenge is identical to the first one, i.e. the same organic compound. Otherwise it is possible to have a substitution of the first vapour and a subsequent earlier breakthrough, in analogy with what happens during the co-adsorption of two or more organic vapours.

Table 1. Comparison of breakthrough times between previously contaminated and re-equilibrated filters and new ones.

Vapour	Filter diameter (mm)	Breakthrough time No prior contamination (min)	Breakthrough time Filter contaminated to about $t_b/3$ Re-equilibration time 6 days (min)	Difference in %
CCl_4	26	53	48	-9
C_6H_5Cl	26	73	71	-3
C_6H_{12}	90	54	55	+2

Another conclusion that can be drawn from these results is the applicability of so-called macroscopic or integral models for the estimation of breakthrough times of organic vapours through activated carbon beds. These models, e.g. the Wheeler-Jonas and derived models, are based on a "total available capacity"-term and a kinetic term (Jonas and Rehrmann, 1973):

$$t_b = \frac{W_e M}{c_{in} Q} - \frac{W_e \rho_b}{k_v c_{in}} \ln\left[\frac{c_{in} - c_{out}}{c_{out}}\right] \quad \text{(Equation 1)}$$

With t_b the breakthrough time [min], W_e the static adsorption capacity [g/g], M the weight of the carbon bed [g], c_{in} the vapour inlet concentration [g/cm^3], Q the volumetric flow rate [cm^3/min], ρ_b the bulk density of the carbon bed [cm^3/g], k_v the overall mass transfer coefficient [min^{-1}] and c_{out} the chosen breakthrough concentration [g/cm^3]. The two unknown parameters in this equation are W_e and k_v. Several authors have established relationships that allow their calculation [10-15] in the case of organic vapour adsorption. W_e is normally estimated (Wood 1992) through the Dubinin-Radushkevich equation (Eqn 2). For organic the value of k_v can be calculated using the semi-empirical equation 4 (Wood and Lodewyckx, 2003):

$$W_e = W_o . d_L . \exp\left[-\frac{B.T^2}{\beta^2} . \log^2\left(\frac{C_S}{C_{in}}\right)\right] \quad \text{(Equation 3)}$$

$$k_v = 800\, \beta^{0.33}\, v_L^{0.75}\, d_p^{-1.5} \left(\frac{W_e}{M_w}\right)^{0.5} \quad \text{(Equation 4)}$$

Where W_e is the static adsorption capacity [g/g], W_o the micropore volume [cm^3/g], d_L the liquid density [g/cm^3], B a structural constant of the carbon, T the adsorption temperature [K], C_s the saturation vapour concentration [ppm], C_{in} the vapour inlet concentration [ppm], k_v the adsorption rate coefficient [min^{-1}], β the similarity constant of the Dubinin-Radushkevich Eqn [-], v_L the linear velocity through the carbon bed [cm/s], d_p the mean diameter of the activated carbon particles [cm], and M_w the molecular weight of the vapour.
The residual capacity, i.e. the first term, can easily be calculated by subtracting the capacity taken by the contaminant from the initial capacity of the filter bed. Example: a pre-contamination during 10 minutes (with the same concentration) by the organic vapour will result in a first term of [$W_eM/c_{in}Q$ – 10 min]. If the concentration or the volumetric flow differ, one should recalculate the equivalent time. The kinetic term is not affected, unless by the loss of capacity (W_e). This loss can easily be calculated by dividing the total mass of pre-contamination by the mass of the carbon bed and subtracting this from th initial value of W_e. Nevertheless, this influence will, in most common types of activated carbon filters, very small ($W_e^{0.5}$!), normally smaller than both the experimental error and the uncertainty of the model.

Conclusions

The tomographic data clearly show a redistribution of a previously adsorbed amount of organic vapour in the filter bed over time. This re-evaporation and subsequent re-adsorption are getting more pronounced when the vapour is more volatile. However, this does not have a marked influence on the future use of the filter under the same circumstances, i.e. against the same vapour. The capacity of a filter can be seen as a conservative quantity: it is not important where in the filter bed the contaminant has been adsorbed, only the total amount of capacity that has been lost. The same reasoning is not valid when the initial contaminant and the new one are different! Furthermore, these conclusions have not been confirmed with very low boiling point compounds and should not be applied to such chemical compounds!

References

Feldkamp, L. A., 1984, Practical cone-beam algorithm, Journal of the Optical Society of America A - Optics Image Science and Vision 1, 612.

Jonas, L.A. and Rehrmann, J.A., 1973. Predictive Equations in Gas Adsorption Kinetics, *Carbon*, 11, 59

Lodewyckx, P. and Vansant, E.F., 1999. The influence of humidity on the adsorption capacity from the Wheeler-Jonas model for the prediction of breakthrough times of activated carbon beds, *American Industrial Hygiene Association Journal,* **60**, 612-617

Sasov, A. and Van Dyck, D., 1998. Desktop X-ray microscopy and microtomography, *J. Microsc.*, **191**, 151-158

Soille, P., 1999. *Morphological Image Analysis – Principles and Applications,* Springer-Verlag, New York

Vinegar, H.J. and Wellington, S.L., 1987. Tomographic imaging of three-phase flow experiments, *Rev. Sci. Instrum.*, **58**, 96-107

Wood, G.O., 1992. Activated Carbon Adsorption Capacities for Vapors, *Carbon*, 30, 593

Wood, G.O. and Lodewyckx, P., 2003. An Extended Equation for Rate Coefficients for Adsorption of Organic Vapors and Gases on Activated Carbons in Air-Purifying Respirator Cartridges, *American Industrial Hygiene Association Journal*, **64**(5), 646-650